



Contents lists available at ScienceDirect

Engineering Science and Technology, an International Journal

journal homepage: www.elsevier.com/locate/jestch



Developing FA-based cementless binder composite by opting sustainable technology: Application of brick and paving block

Minkwan Ju^a, Khuram Rashid^b, Idrees Zafar^{c,*}, Mounir Ltifi^{c,d}

^a Department of Civil and Environmental Engineering, Yonsei University, Seoul, Republic of Korea

^b Department of Architectural Engineering and Design, Faculty of Civil Engineering, University of Engineering and Technology, Lahore, Pakistan

^c Department of Civil Engineering, Imam Mohammad Ibn Saud Islamic University, Riyadh, Saudi Arabia

^d Department of Civil Engineering, National Engineering School of Gabes, University of Gabes, Tunisia



ARTICLE INFO

Keywords:

Alkali activated binder
Dune sand
Physico-mechanical performance
Multi-criteria decision making
Brick and Paving Block

ABSTRACT

Cementless binders are made possible by the invention of geopolymers, which utilize alkaline activators to activate alumina-silicate materials. Alkaline activators, however, are corrosive and hazardous. Its minimal usage combined with advanced technology can make it sustainable. Therefore, this work was designed to develop alkali-activated binders (AABs) through mechano-chemical activation. Initially, three types of fly ashes (FAs) were activated, and their performance was evaluated using the strength activity index. The best-performing FA was used in the second group of experiments. Slag was coupled with FA, and dune sand (DS) was coupled in the third group. The physico-mechanical performance of each group was evaluated and the geopolymerization mechanism was assessed through FTIR analysis. By using DS, it was observed that the compressive strength has been significantly enhanced with an increase of 100 % compared to the FA-based binder, while the bulk density of both cases is almost the same (i.e., 1,650 kg/m³). Based on the multi-criteria analysis for three scenarios, it is revealed that the key performances of the high strength and durability, the lightweight and insulation, and the strength requirement are optimized by alkali-activated binders of FA + DS, FA-3, and FA + GGBS (Slag), respectively.

1. Introduction

Geopolymers have been extensively studied from the last two decades and is broadly grouped into two types, one-part and two-part geopolymers by alkali-activated process [1,2]. Both types contribute to achieve sustainable development goals defined by UN., and specifically form part of UNEP White Paper Group of Eco-Efficient Cements. The well-formulated mix design and activation of alkali-activated binders (AABs) by appropriate means make it cost effective and environment-friendly [3]. However, priority is given to one-part geopolymers or alkali activated binder (AAB) over two part [4], as in two part alkaline activator is used in liquid form by labour and these activators are considerably hazardous for human health and safety when they are manually handled. Contrary to this, AAB has widely applicable at industrial scale and all activation methods and final products in powder or binder form will be available for customer. Only the least amount of water is required to complete the geopolymer mixtures. Since

ambient and hot curing condition is recommended for geopolymers, and such environment is natural in the arid regions. Some novel researchers have tried to physically optimize the geopolymer mixtures by parametric study using factors such as FA/Slag ratio, curing temperature [5–7]. However, for optimizing design of one-part geopolymer mixture, a comprehensive scientific decision analysis should be employed as well as physical performance assessment.

One of novel natural precursor is dune sand (DS), which is infinitely provided in arid region. According to ASTM and AASHTO soil classification system, it is classified as SP, i.e., poorly graded sand. Classification is provided for different locations (13 locations) of the world and almost all types were SP [8]. Its fineness modulus value is low (0.45–1.00) [9,10], whereas for river sand the values vary from 2.45 – 2.65 [11]. Therefore, poor grading, fine grain size, rounded shape and negligible plasticity make it unfit for conventional construction purposes. An effort has also been made to replace the conventional aggregate by using expanded clay [12]. Thus, technical trials have been made

* Corresponding author at: Department of Civil Engineering, College of Engineering, Imam Mohammad Ibn Saud Islamic University, P.O. Box 5701, Riyadh 11432, Saudi Arabia.

E-mail addresses: j_dean21@yonsei.ac.kr (M. Ju), khuram_ae@uet.edu.pk (K. Rashid), izsatti@hotmail.com (I. Zafar).

<https://doi.org/10.1016/j.jestch.2023.101580>

Received 18 June 2023; Received in revised form 24 October 2023; Accepted 9 November 2023

Available online 21 November 2023

2215-0986/© 2023 Karabuk University. Publishing services by Elsevier B.V. This is an open access article under the CC BY-NC-ND license (<http://creativecommons.org/licenses/by-nc-nd/4.0/>).

Table 1

Summary of alkali-activated binder and 28 d strength in recent years.

No	Precursors	Activators	Activation	Calcination	Curing	Comp. Strength* (MPa)	References
	Lithium Slag, GGBS	Na ₂ SiO ₃ -anhydrous	No	No	A ¹	57	[24]
	GGBS	Na ₂ SiO ₃ -anhydrous	No	No	A	90	[34]
	Fly Ash	Na ₂ SiO ₃ , NaOH	No	No	40 °C	65	[35]
	Fly Ash, GGBS	Ca(OH) ₂ , NaOH, Na ₂ SiO ₃	No	No	60 °C	37	[36]
	Rice Husk Ash	NaAlO ₂	No	650 °C	80 °C	33 at 3 d	[37]
	Fly Ash, GGBS	NaOH, Na ₂ SiO ₃ , Na ₂ CO ₃	No	No	A	51	[38]
	High Calcium Fly Ash	Na ₂ SiO ₃ -anhydrous	No	No	A	50	[39]
	Fly Ash, GGBS	Na ₂ SiO ₃ anhydrous, Na ₂ CO ₃	No	No	A	66	[40]
	Fly Ash, Bottom Ash	Na ₂ SiO ₃ , NaOH	Mechano-Chemical	No	65 °C	95 at 7 d	[25]
	Coal Fly Ash	CaO, MgO, NaOH	Mechano-Chemical	No	A	35	[26]
	Cement Kiln Dust, Feldspar	Na ₂ CO ₃	Thermo-Chemical	1,300 °C	A	38 at 7 d, 52	[27]
	Fly Ash, Bagasse ash	Na ₂ SiO ₃ anhydrous,	Mechano-Chemical	No	70 °C	15.8 at 7 d	[41]

A¹ = ambient curing condition, * strength at 28 d.

to use it in conventional concrete, but reduction in the mechanical strength had been observed with the addition of DS [13–15]. The usage of DS was from 0 – 100 % and the corresponding strength reduction was resulted in 14.3 % [9]. It is noted that that DS is industrially discarded as the fine aggregate of the structural concrete. However, for AABs, the high fineness of DS may pay vital importance in geopolymmerization and strength development. Furthermore, the richness in silica of DS and high surface area may make it compatible for the development of tetrahydron structure of one-part alkali activated components. There was an attempt to make a one-part geopolymers mixture using unique component [16], thus, more extensive study still needs for carbon neutral geopolymers cement.

Several types of alumino-silicate materials have been utilized to formulate geopolymers, broadly, it was divided into low and high calcium precursors [17]. Fly ash (FA), which has extensively been investigated to develop geopolymers, is usually low-calcium precursor, and high curing temperature is recommended for its curing. The leaching of alumina and silica expedite after 65 °C and therefore hot curing condition is recommended for FA-based geopolymers for early strength [18,19]. A comprehensive summary has been prepared in which thermally insulated concrete performance has been reported [20]. Along with the reactivity of the precursors, the other factors that influence the mechanical strength of the two-part geopolymers are type of precursor, the alkaline to precursor ratio, ratio between alkaline activators (Sodium Silicate/Sodium Hydroxide (Na₂SiO₃/NaOH)), molarity of NaOH solution) and curing temperature etc. [21].

However, their correlations with the strength are well documented for the targeted compressive strength of FA-based geopolymers [21,22]. But still the reactivity of the FA is the crucial step and relation of mechanical strength with the reactivity of precursor has also been reported [19]. Another precursor, ground granulated blast furnace slag (GGBS), is the high calcium precursor, and dissolution of alumina and silica from GGBS occurred at faster rate at ambient condition as compared with the high temperature condition [23]. Therefore, for ambient curing, slag-based geopolymers are being developed [2,24]. Table 1 summarized the type of precursors used for the development of AAB and their corresponding compressive strengths. To extensively use the by-product for replacing cementitious materials, the combination of FA and GGBS can realize the eco-friendly construction members such as masonry and bricks.

The reactivity of FA is vital to one-part geopolymers or AABs, and the mechano-chemical activation [25,26] and thermal activation [27] of FA have been applied. For thermal activation, a calcination temperature of 350–1,500 °C has been applied to achieve better performance [1]. The chemical reactivity of precursor resulted in the formation of one-part geopolymers [22], fusing alumino-silicate material with NaOH solution activate the material and formed the alkali activated binder. The Table 1 summarized the AAB along with the activation method used. However, the sustainability of fabrication with respect to energy consumption remains questionable. The FA has also been used to improve the soil

properties for the pavement and is capable to reduce the plasticity [28]. The FA was also used to enhance the performance of grout [29]. The FA was also activated by CaO and improvement in the compressive strength has been observed [30]. Along with that, it has been used with agricultural waste to produce construction material like brick [31]. The advantage of pressing on precast concrete bricks, pavers, and kerb stones is evident. By applying uniaxial pressure, air voids are removed, which renders the paste dense. In fact, this is the most important aspect in geopolymers. The uniaxial pressure can further activate the aluminosilicate materials, and almost all particles are wetted by the alkaline solution; consequently, the mechanical strength is increased [32]. Among the previously applied molding pressures (10–60 MPa), 20 and 40 MPa yielded the optimal mechanical performance for FA-based geopolymers and clay [32]. Meanwhile, for FA-based geopolymers only, a molding pressure of 20 MPa was adequate for the formulation of masonry bricks [33].

In this study, a novel and systematic approach is employed to formulate an alkali-activated binder (AAB) through mechano-chemical activation. The performance of construction bricks incorporated with AABs is then investigated. It has been extracted from Table 1 that the alumina-silicate material is activated by an alkaline activator, and only a few studies are available where thermomechanical and mechanochemical techniques were used. Moreover, the suitable combination of FA with GGBS and industrially discarded sand (dune sand (DS)) is missing. Therefore, this study was designed to use three types of FA with different particle size distributions obtained from various sources, including GGBS and DS, as precursors. The physical properties, such as density and water absorption, as well as the mechanical performance, specifically compressive strength, of the three precursors, are being investigated. In Group-I, the most reactive FA is determined. Group-II comprises the selected FA from Group-I and the GGBS combination for geopolymers. Finally, Group-III comprises the selected FA geopolymers mixture incorporated with a rich-silicate DS as a precursor. The inherent physico-mechanical properties of these categories are evaluated according to the established performance criteria for masonry bricks and paving bricks. Additionally, this paper presents an application of geopolymers mixtures that focuses on their manufacturing performance in arid regions.

2. Experimental methodology

2.1. Materials

For the development of AAB, the materials used in this study are fly ash (FA), ground granulated blast furnace slag (GGBS) and dune sand (DS), which were activated. FAs were obtained from three industrial sources. FA-1 was obtained from the paper industry, whereas FA-2 is from a coal power plant, which was designed solely for electricity of cement plant (DG Khan Cement Private Limited) in Pakistan. And FA-3 is also from another coal power plant where it has generated 1,300 MW

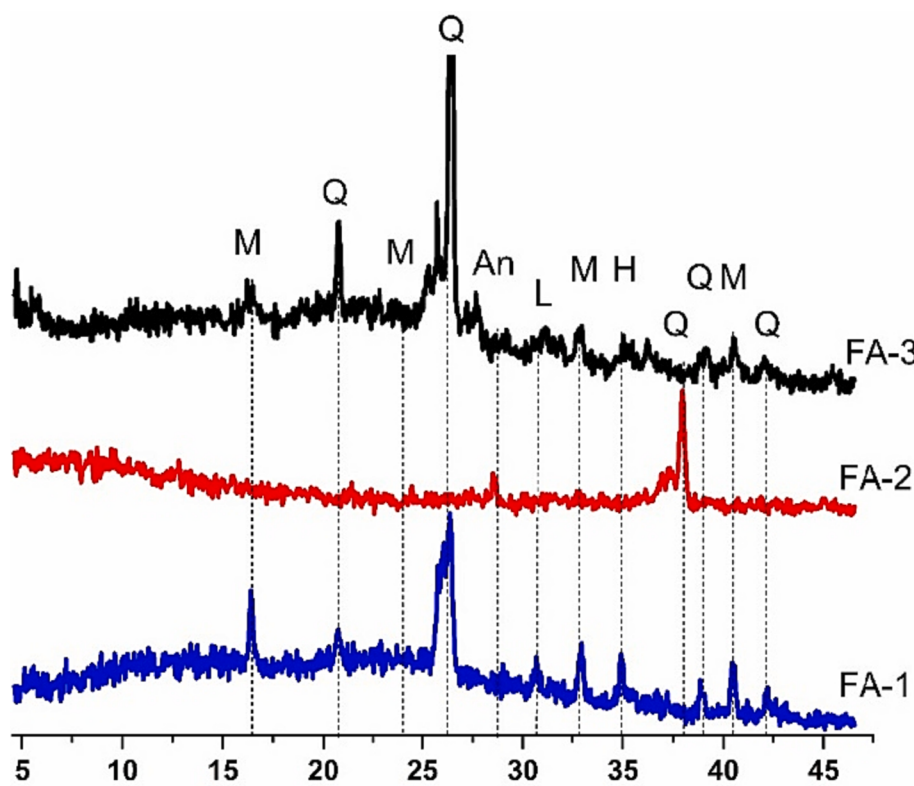


Fig. 1. X-ray diffraction analysis of all types of FAs used in this work (A = Anhydrite (CaSO_4), M = Mulite, Q = Quartz, H = Hematite, L = Lime).

Table 2
Chemical composition of precursors used in this work (unit in %).

Material	CaO	SiO_2	Al_2O_3	MgO	SO_3	Fe_2O_3	K_2O	Na_2O	LOI
FA-1	9.0	56.3	23.1	1.7	–	6.4	0.6	0.3	< 3
FA-2	4.8	54.1	28.2	0.9	0.7	4.9	0.6	0.1	–
FA-3	6.5	51.7	16.5	1.5	2.2	4.6	–	–	4.1
GGBS	40.9	37.4	13.3	1.6	0.6	1.3	0.0	0.4	2.3
DS	4.7	67.4	11.8	2.1	0.0	6.5	1.5	2.4	–

capacity of industrial electricity. The X-ray diffraction (XRD) analysis of all types of FAs is shown in Fig. 1. It has been observed that FA-1 and FA-3 have many peaks, and the corresponding mineral has also been presented in Fig. 1. GGBS is the grade 80 slag and its maximum particle size was $75 \mu\text{m}$ [42]. DS was obtained from desert which indicate abundance of materials, it is poorly graded and average grain size, “ D_{50} ” is 0.2 mm. The chemical compositions of all solid precursors are provided by XRF analysis as presented in Table 2. It was observed that all types of FAs are low calcium and Class F FA according to ASTM C618 [43]. The GGBS is the high calcium precursor which is capable to be activated at ambient condition. DS has the highest amount of silica components among the precursors. Fig. 2 describe the summary of oxides present in each material as well as compared with supplementary cementitious materials. It has been observed that GGBS is rich in CaO, and FAs are rich in SiO_2 and Al_2O_3 .

The other solid materials are alkaline activators and combination of sodium hydroxide (NaOH) and sodium silicate (Na_2SiO_3) are used. Both activators are commercial products. The NaOH was available in pellet form, whereas Na_2SiO_3 was available in powder form and color of both activators is white as shown in Fig. 3.

2.2. Specimen preparation

In the experimentation, three types of FAs were investigated. Based on their physical-mechanical performance, one FA was selected for

further investigation. It was coupled with the GGBS to ensure the desired performance under ambient curing conditions. Furthermore, the amount of FA and activator was reduced by adding industrially discarded sand (DS), which may result in improved packing and activation of FA. Therefore, this work was divided into three groups and explained as follows.

In Group-I, all types of FAs are mechanically mixed with Na_2SiO_3 powder and NaOH pallet. Different trials are used to set the ratio of Na_2SiO_3 to NaOH, the reported range for this ratio is varies from 1.0 – 8.7 [21], and in this work 5.3 ratio is employed. The amount of FA and other constituents has been mentioned in Fig. 4. The mixing of all constituents is carried out by high-speed mixer to further increase the fineness of resultant AAB. In the same mixing pan, low ratio (0.2) of water to solid (binders or sand) (W/S) is employed. Semi-dry paste is intended to maintain the cylindrical shape in the cylindrical steel mold after the uniaxial pressure of 20 MPa (Fig. 3).

However, in the case of FA-3 specimen, a slurry is formed at a water to solid (w/s) ratio of 0.2. Therefore, it was reduced to 0.1 in order to maintain a cylindrical shape (Table 4). The casting and pressurized cylinder specimens are demolded immediately. They are developed through a chemical interaction of precursors with alkaline activators during mechanical mixing. Then, uniaxial pressure is applied to develop cylinder specimens with a diameter of 50 mm and a length ranging from 90 to 100 mm. The fabrication process of the specimen preparation to develop AAB and the final product is shown in Fig. 3. Finally, they are

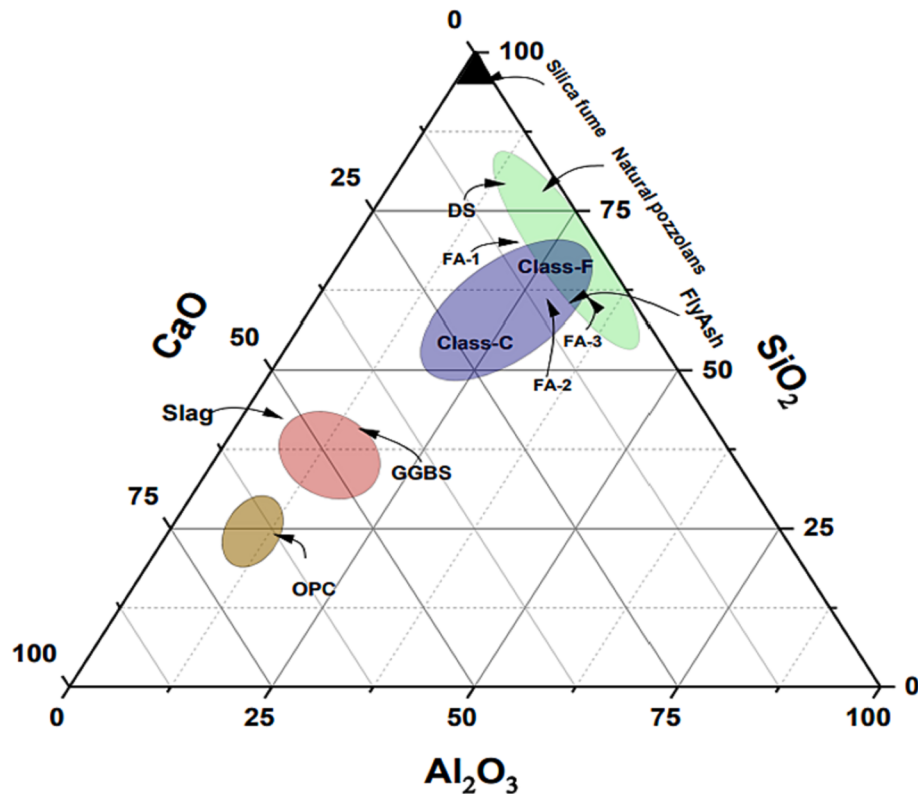


Fig. 2. Main oxides presented in FA, GGBS and DS.

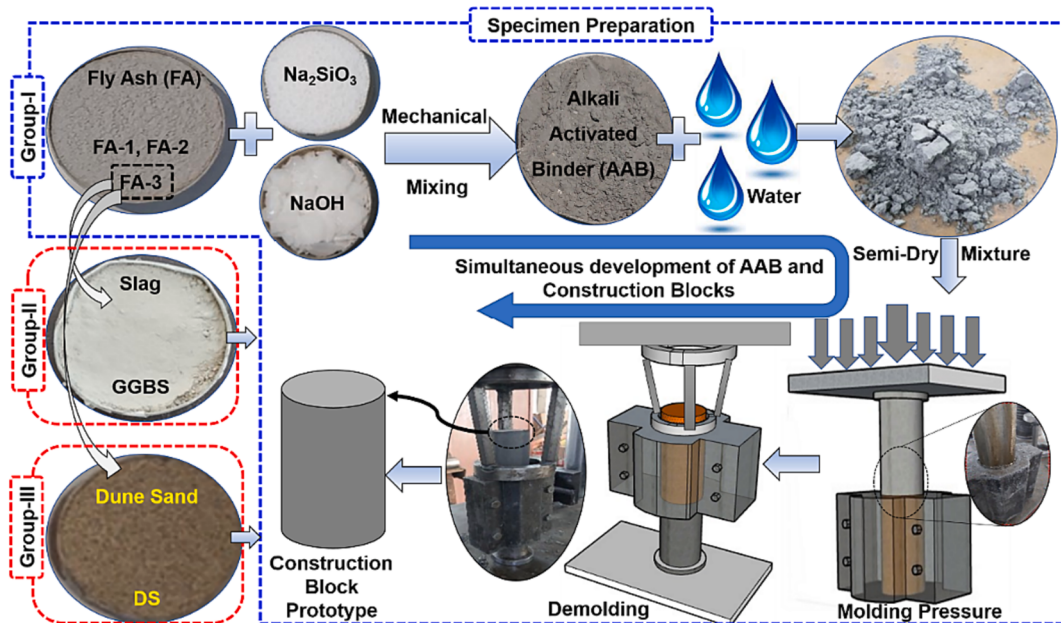


Fig. 3. Methodology of developing AAB and construction brick.

wrapped in a polythene sheet and placed in an oven at 70 °C for 24 h for hot curing. For FA-based geopolymer, the hot curing condition is prefer and 70 °C temperature has been optimized for its adequate reactivity [21]. Another mixture groups (Group-II and Group-III) are designed after optimizing the type of FA from Group-1, GGBS and DS were used in Group-II and Group-III, respectively.

The mix proportioning is presented in Fig. 4 and the particle size distribution of AAB and DS is mentioned in Fig. 5. In Group-II, the

optimized FA was replaced with GGBS by an amount of 20 %wt. (Fig. 4), to obtain the mechanical strength at ambient curing condition, instead of hot curing condition. The GGBS is high calcium precursor and need ambient condition for its dissolution in alkaline environment [44]. For Group-III, GGBS was replaced by DS (Fig. 4), by an amount of 20 %wt. For hot curing condition, 2 h at 100 °C for 24 h and 200 °C for 2 h are applied as recommended for desert sand [45]. Then the specimens are covered by polythene sheet and cured at ambient condition until testing

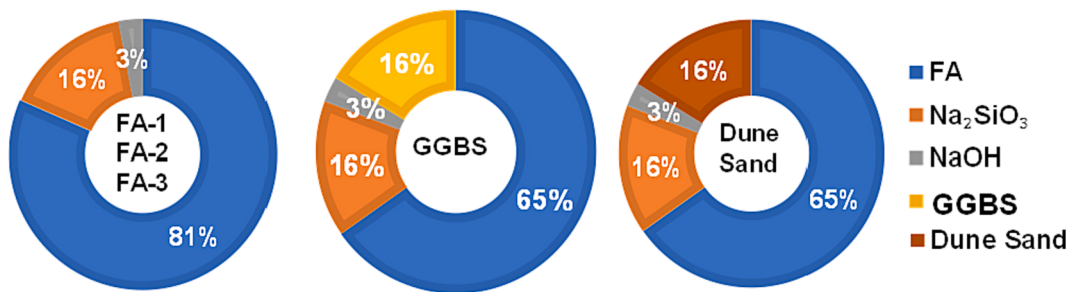


Fig. 4. Mix proportion of mixtures used in three groups.

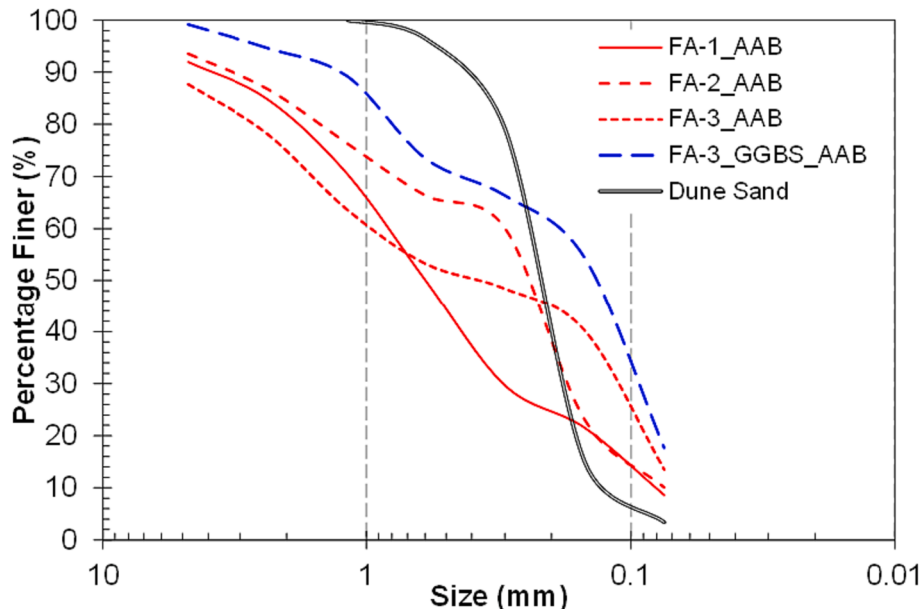


Fig. 5. Sieve analysis of dry mix alkali activated binders and dune sand.

Table 3
Mixture group and curing conditions.

Group	Precursors	w/s ^a	Curing		Samples ^c	
			Hot °C	Ambient °C	7 d	28 d
Group-I	FA-1	0.2	70	–	3	3
	FA-2	0.2	70	–	3	3
	FA-3	0.1	70	–	3	3
Group-II	FA-3 + GGBS	0.1	–	25	3	3
Group-III	FA-3 + DS	0.1	100 + 200 ^b	–	3	3

w/s^a = water to solid ratio; 100 + 200^b = 2 h at 100 °C then after 24 h further curing at 200 °C for 2 h; Samples^c = compressive strength, water absorption and bulk density.

age of 7 and 28 d. The fabrication process of Group-II and Group-III is same with Group-I and summarized in Fig. 3. The summary of all groups has also been enlisted in Table 3.

2.3. Testing

Physical property is investigated by bulk density test [46], where the weight and volume of the specimen are noted before its crushing, and the ratio of weight to volume depicts the bulk density. The water absorption, another physical property, was calculated by taking the difference between the saturated and oven-dried specimens. The oven drying was carried out for 24 h at 105 °C. The water absorption test was carried out by following the standard guidelines [47]. The compressive

strength test is conducted according to ASTM C109 [48]. Three cylindrical samples are tested for each mixture and their average value is reported as the compressive strength in this work. Mixture group details are introduced in Table 3. The Fourier transform infrared (FTIR) spectroscopy was also carried out to evaluate the degree of geopolymers. After compressive strength test, the specimen is further crushed into the particles and the FTIR analysis is conducted using few grams of the particles. The Analysis is performed by Bruker Compact FTIR spectrometer with a range of 500–4,000 cm⁻¹.

3. Results and discussion

3.1. Effect of reactivity of FA

For geopolymers, several other factors (Alkaline to precursor ratio (A/P), Na₂SiO₃/NaOH (SS/SH), and molarity of NaOH solution) affect the compressive strength. Therefore, in this study, all parameters were incorporated and set to constant values, except for those of FA. The compressive strengths after 7 and 28 d are presented in Fig. 6. The result shows that FA-1 and FA-3 exhibited the lowest and highest reactivity, respectively. Quantitatively, the difference between them was approximately 88 %, which corresponded to a variation in the compressive strength by 9.6 to 22.7 MPa. Moreover, the difference between the 7 and 28 d compressive strengths was marginal for FA-2 only, which is attributable to the greater fineness of FA-2, as shown in Fig. 5. Almost 60 % of the particles varied from 0.15 – 0.30 mm. The high fineness accelerated geopolymers due to the larger surface area, and the

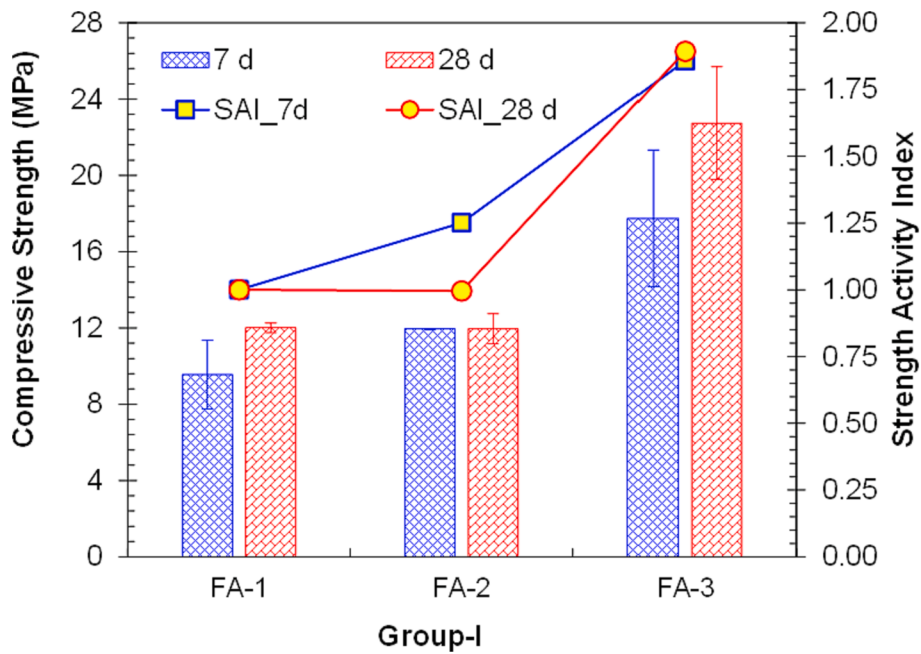


Fig. 6. Compressive strength of specimens of Group-I.

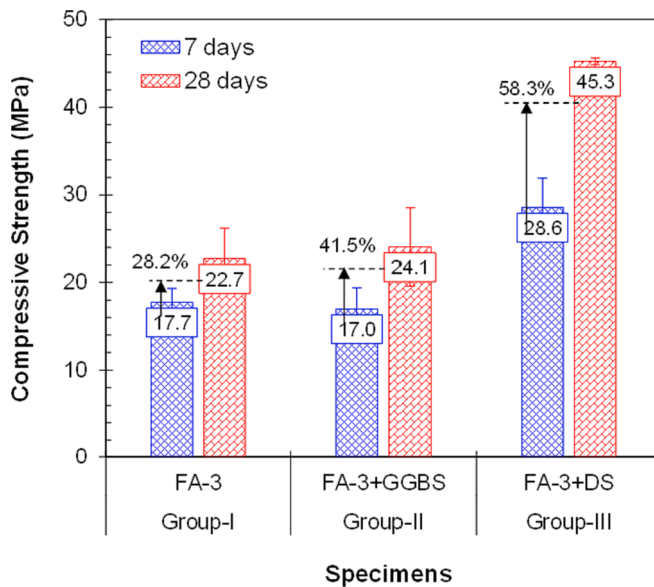


Fig. 7. Summary of compressive strength of all specimens (Group-I – Group-III).

process was completed within 7 d. For FA-1 and FA-3, the difference in the compressive strengths at 7 and 28 d was 25.7 % and 28.2 %, respectively. FA-based geopolymers exhibit early strength due to hot curing. However, their strength can be further improved over time by addressing the variation in particle size.

The strength activity index (SAI) was calculated by normalizing the value with respect to the compressive strength of FA-1. Notably, the SAI value is defined in ASTM C311 [49]. Based on Fig. 6, the SAI value was 1.25 and 1.86 at 7 d, which indicates an increase in the compressive strength of 25 % and 86 % for FA-2 and FA-3, respectively, as compared with FA-1 (Fig. 6). At 28 d, the increment in SAI value (1.89) for FA-3 was similar to that observed at 7 d. However, the SAI value of FA-2 decreased because of the similar strength of FA-2 at both 7 and 28 d.

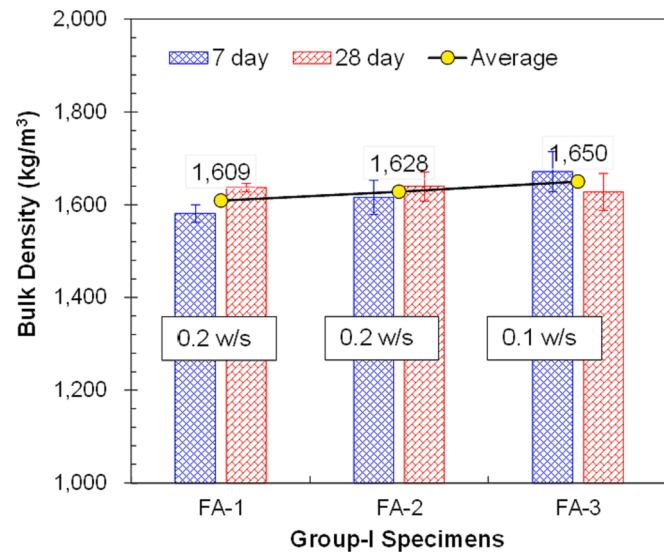


Fig. 8. Bulk density of all specimens of Group-I.

3.2. Compressive strength comparison

A summary of the compressive strength of the specimens from Groups I to III is shown in Fig. 7. The strength obtained by partially replacing FA-3 with GGBS obviated the necessity for hot curing and yielded almost the same compressive strength across all groups. GGBS is a high-calcium precursor that is more reactive under ambient conditions than under hot curing conditions. The reactivity of GGBS was investigated via a dissolution test, and the result shows that GGBS is more reactive under ambient conditions [19]. Therefore, the compressive strength observed at 28 d was 41.5 % higher than that observed at 7 d. However, FA-3 indicated only a 28.2 % increase in compressive strength. Additionally, DS was added as a precursor instead of merely a filler, and a promising response was observed, as shown in Fig. 7. The compressive strength indicated by Group-III was more than 60 % higher

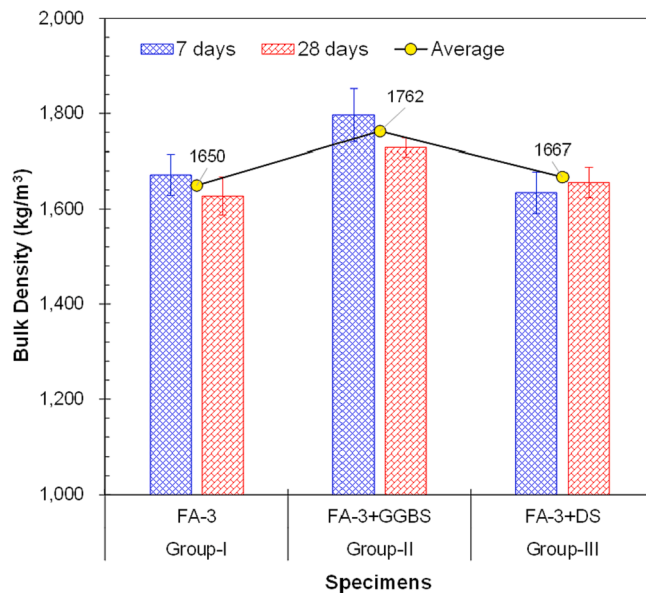


Fig. 9. Summary of bulk density of all types of specimens (Group-I – Group-III).

than that exhibited by Groups I and II. This is attributable to the fineness of DS and the filling of pores in its dense structure. Furthermore, the crystalline structure of DS allows it to bear more load; under pressure, FA can be pressed and its cenosphere can be damaged, whereas DS remains as a solid, bears the load, and renders the FA more reactive. Furthermore, the increase in compressive strength with age exhibited by Group-II was more extensive compared with that of Groups I and II.

3.3. Effect of bulk density on lightweight property

The average bulk density of the AAB mixtures was calculated at 7 and 28 d and is presented in Fig. 8. The density was measured to be 1,609–1,650 kg/m³, which is much lower than that of normal concrete (2,200–2,400 kg/m³) and brick masonry (1,800–2,000 kg/m³). Thus, the lightweight property was demonstrated, and the difference in density among the three types of FA was minimal. This implies that curing has been completed and all hydration products, either calcium-alumino-silicate-hydrate (C-A-S-H) or sodium-alumino-silicate-hydrate (N-A-S-H) gels, might have already formed due to hot curing. This is because the decrease in the water to solid (binders or sand) (w/s) ratio increased the bulk density, which in turn increased the reactivity of the AAB. As a result, the hydrated products became denser. However, the difference was marginal due to uniaxial pressure [50].

The cold binding of the material, caused by the molding pressure, reduced the air void content and generated dense microstructures. This, in turn, led to an increase in the density [33]. Furthermore, water in the voids was removed through hot curing, which reduced the density. Consequently, the average bulk density measured for the FA specimens was 1,630 kg/m³, which was confirmed to be much lower than that of normal concrete.

Fig. 9 shows the bulk density of the mixture group at 7 and 28 d. FA-3 was selected in Group-I due to its highest reactivity and high compressive strength, as explained in Section 3.1. The bulk density increased when GGBS and DS were used in the FA-3 mixture. Notably, FA particles are spherical and hollow, containing cenospheres [51]. As a result, specimens made up of FA particles have a lower bulk density compared to specimens made up of denser particles like GGBS and DS.

The bulk density of the specimens in Group-II was relatively high owing to the presence of GGBS; moreover, the specimens in Group-II were cured in ambient temperature, where water remained and occupied all voids, thus resulting in an increase in the bulk density. The bulk

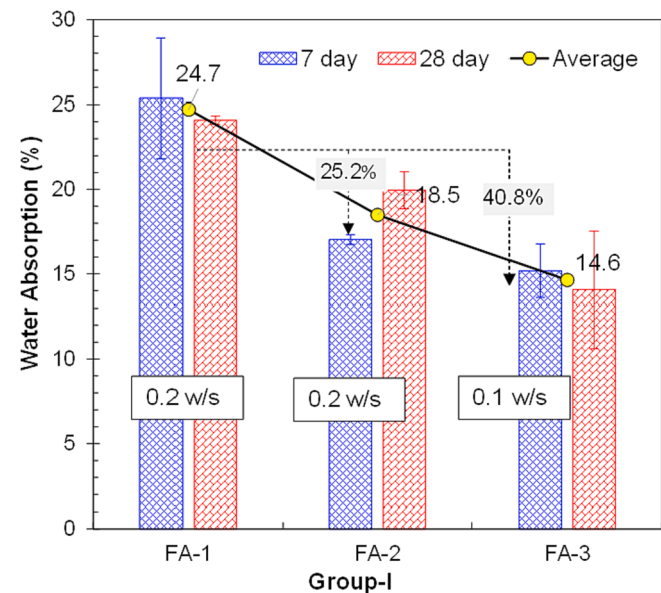


Fig. 10. Water absorption of all specimens of Group-I.

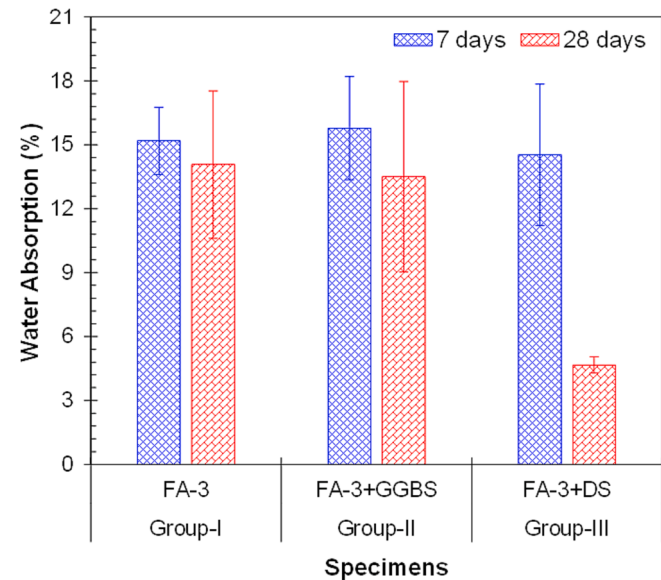


Fig. 11. Summary of water absorption of all specimens (Group-I – Group-III).

density of this group, which ranged from 1,650 to 1,762 kg/m³ was much lower than that of conventional mortar or concrete; hence, the specimens in this group exhibit high potential to be used as lightweight construction brick members.

3.4. Effect of water absorption on insulation performance

The measured amount of water absorbed by the three types of FA-based geopolymer material at 7 and 28 d is shown in Fig. 10. The effect of age was marginal; however, the average amount of water absorbed decreased from FA-1 to FA-3. Meanwhile, the water absorption decreased as the bulk density increased.

This was caused by the change in the FA type to one with a low water-to-solid ratio and that most of the voids were filled with fine FA particles, thus resulting in a decrease in water absorption. Furthermore, FA-3 contained a significant amount of amorphous silica (Fig. 1) and was able to react and form gels such as C-A-S-H and N-A-S-H gels,

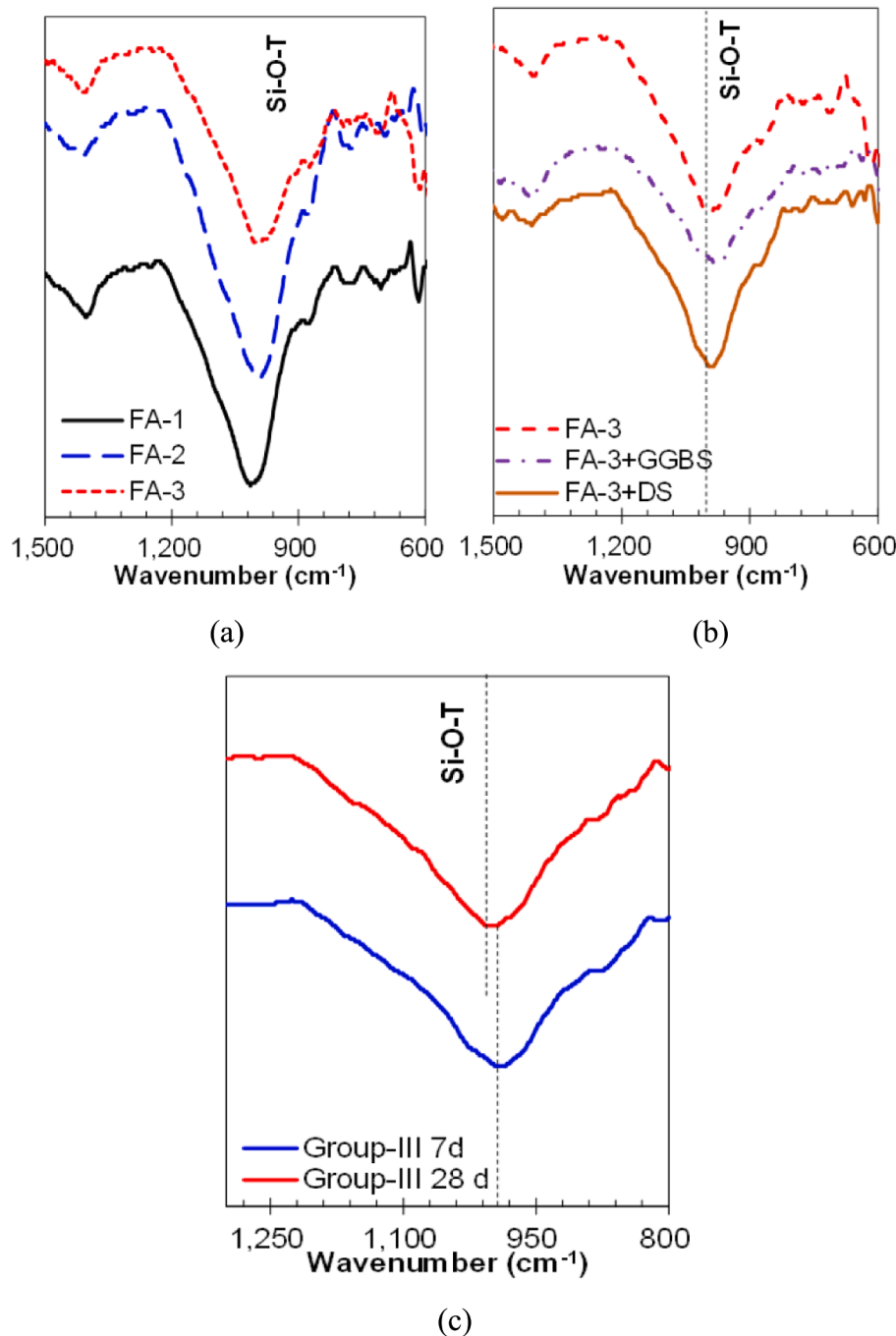


Fig. 12. FTIR curves of all specimens: (a) Group-I, (b) Group-I to III, and (c) DS incorporated.

thereby preventing water absorption. Therefore, FA-3 demonstrated the lowest water absorption, with a maximum reduction in bulk density of 40.8 %.

Fig. 11 presents the measured water absorption of FA-3 and its composite with GGBS and DS in Groups I, II, and III, separately. The water absorption at 7 d was marginal; however, Group-III indicated the most significant reduction at 28 d. The difference between the Group-I specimens at 7 and 28 d was marginal (7.3 %) under the hot curing condition, in which FA activation was completed at the early ages. For Group-II (with GGBS), the water absorption at 28 d did not differ significantly to that of Group-I. Thus, ambient curing with GGBS can result in slightly less water absorption without high energy consumption. As GGBS is rich in calcium and the ambient curing condition is sufficient for the formation of C-A-S-H gel, water absorption can be

prevented. In the Group-III specimens based on DS, the water absorption at 28 d reduced significantly by 67.9 % as compared with that at 7 d. Furthermore, at 28 d, porous less microstructures were generated during the hot curing state, which was not observed at 7 d. Group-I of FA-3, Group-II, and Group-III indicated acceptable results, i.e., water absorption of less than 15 %, based on building brick specifications [52]. The porous microstructure provided better insulation against heating and cooling [53]. Researchers have incorporated different materials to create porous material structures without compromising the strength [54]. In arid regions, the temperature increases to 60 °C in the summer [55], which allows formulated products to function better owing to the porosity afforded.

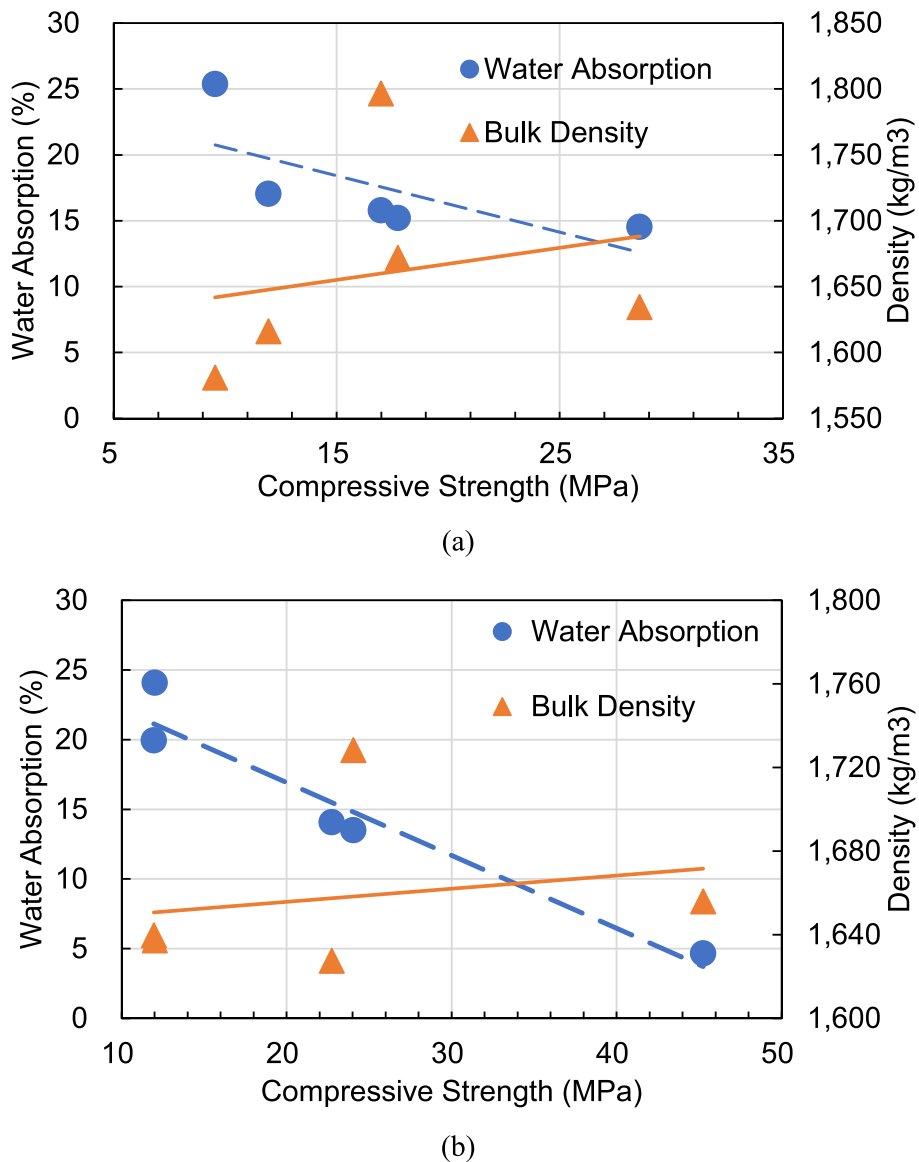


Fig. 13. Physico-Mechanical relationships of specimens at: (a) 7 d and (b) 28 d.

3.5. FTIR analysis

FTIR analysis is carried out after performing a 7 d compressive strength test, and the FTIR curves of the specimens from Group-I are shown in Fig. 12. It can be observed that the rate of geopolymerization is almost the same for all types of FAs, as Si-O-Si or Si-O-Al (generally expressed as Si-O-T) have almost the same wavenumber. However, the different depths of curves can be seen as peaks, and the area under the curve indicates the rate of geopolymerization [56]. The Si-O-T peaks are almost at the same wavenumber, but obviously, different mechanical strength is measured as described in Section 3.2. The rate of geopolymerization for all types of AAB is almost the same. Although the area under the curve is slightly different, it may be correlated with the strength [57]. Furthermore, this behavior is exhibited through dehydroxylation and may result in an increase in compressive strength. That can be verified from the difference in strength between Group-III specimens with and without DS incorporation (Fig. 7).

The FTIR curves are indicated in Fig. 12. Although there are some differences in the peaks, it can be concluded that these differences are marginal. The significant difference in strength is attributed to the physicochemical processes occurring on the specimen, resulting in

evaporation and dehydroxylation. Moreover, it is caused by the physical characteristics of the developed AAB mixture and their relationship with the compressive strength, as described in the following Section 3.6.

3.6. Physico-mechanical relationship

The relationship between the physical properties of bulk density and water absorption, as well as the compressive strengths at 7 and 28 d, as shown in Fig. 13. The compressive strength and water absorption show a strong correlation. Therefore, a decrease in water absorption leads to an increase in compressive strength. This is a common physico-mechanical phenomenon observed in dense microstructures. The results for the Group-I specimens, based on FA-3, show that at 28 d, the compressive strength increased as the density decreased. However, the specimens based on FA-1 and FA-2 were lightweight but did not meet the required structural strength. Thus, the specimen based on FA-3 can be made lighter, with a moderate increase in strength. Groups II and III showed that the addition of GGBS and DS resulted in an increase in the bulk density of the hydration products at 28 d. Group-II, which is based on GGBS, indicated a higher density than the FA-based mixtures. This is because ambient curing does not allow a significant amount of water to

Table 4
Performance-based scenarios of geopolymmer construction brick.

Scenarios	Description	Physico-Mechanical Performance		
		Bulk density	Water absorption	Compressive strength
Scenario-1	High Strength of Durability	Max	Min	Max
Scenario-2	Lightweight of Thermal Insulation	Min	Max	Min
Scenario-3	Strength Requirement	Min	Min	Min

evaporate rapidly.

Thus, the results reconfirmed that the bulk density changed slightly from 7 to 28 d. Meanwhile, the specimens in Group-III, based on DS, indicated a significant improvement in strength, even though their bulk density was similar to that of the FA-based mixtures. Therefore, high-strength and lightweight materials can be achieved using AABs incorporated with DS in arid regions. However, good decisions cannot be made based solely on the physico-mechanical performance. Hence, we will discuss the standards for bricks as well as their performance in the following [Section 4](#).

4. Performance-based design assessment

4.1. Performance scenario

To investigate the performance-based design of AAB bricks for construction, the physico-mechanical performance of the cylindrical specimens is being investigated. Based on the performance results, multi-criteria decision making (MCDM) analysis is used to recommend the optimal AAB mixtures based on the performance-based scenarios. The physico-mechanical performance is classified into three categories: lightweight, high strength, and required strength. Thus, it mainly comprises fundamental properties (bulk density, water absorption, and compressive strength) that are investigated and reported in codes for the selection of any product, such as brick masonry, concrete brick, kerb stones, or pavers [52,58]. It is obvious that an increase in bulk density promotes mechanical strength. However, it also results in an increase in the dead load of the structure. It is noted that achieving a decrease in bulk density without compromising mechanical strength is the ideal application for lightweight products made of AAB. Similarly, water absorption is strongly related to mechanical strength. Higher water absorption results in lower strength, and vice versa. However, high water absorption is strongly related to the high porosity of the microstructure of materials, which contributes to their good insulation properties in arid regions. A lot of efforts have been made to incorporate various fibers [53], and design concrete bricks that are insulated for hot climatic conditions, where the environmental temperature usually rises up to 60 °C [55]. Another important aspect is strength. For high strength in arid regions, it is a significant issue to use rich-silicate DS as a fine aggregate in the AAB mixture for structural construction bricks. The minimum required strength for the construction brick can also be important from an economic standpoint when using an AAB mixture. This strength criterion is designed to recommend cost-effective construction bricks for use in designated areas with minimal external stress, particularly in arid regions. It is also a fact that a large quantity of structural material is required for masonry work or partition walls in frame structures. Accordingly, this study has reasonably established three performance scenarios for the geopolymmer construction bricks, as summarized in [Table 4](#).

The higher strength is achieved through an increase in bulk density, resulting in strong and durable AAB mixtures. Thus, it is set as Scenario-1 described as "High Strength and Durability". The materials with high porosity in their microstructure result in lower bulk density and high

insulation capacity. This Scenario-2 is described as "Lightweight Thermal Insulation". Finally, for cost-effective application, the required strength of structural materials is set as Scenario-3, based on the strength requirement of bricks or brick masonry, with a strength of 10.3 MPa according to ASTM C62 [52]. In each scenario, there are three aspects of physico-mechanical performance that are considered. A comprehensive summary of the qualitative values for each scenario is presented in [Table 4](#).

4.2. Multi-criteria decision-making analysis

For different scenario and different criteria make the system complex and for simplicity or automated selection, the MCDM technique is employed. Therefore, Technique for order preference by similarity to ideal solution (TOPSIS), widely opted for selection of sustainable construction materials [11,23,59] is utilized in this work. Followings are the processing steps of the TOPSIS.

4.2.1. Step-1: Establishment of decision matrix

It was established by incorporating all alternative (for each scenario) along with their corresponding criteria. Eq. (1) describes the generalized form of decision matrix (DM), x_{ij} is the performance value of i^{th} alternative with respect to j^{th} criterion ([Table 2](#)).

$$DM = [x_{ij}]_{m \times n} = \begin{bmatrix} x_{11} & x_{12} & \cdots & x_{1n} \\ x_{21} & x_{22} & \cdots & x_{2n} \\ \vdots & \vdots & \ddots & \vdots \\ x_{m1} & x_{m2} & \cdots & x_{mn} \end{bmatrix} \quad (1)$$

4.2.2. Step-2: Normalization of decision matrix

Next step is the normalization of the values of all criteria and the influence of unit (e.g., MPa, kg/m³, and %) vanished by the normalization and all values ranged from 0 – 1. DM matrix can be normalized by following Eq. (2).

$$P_{ij} = \frac{x_{ij}}{\sum_{i=1}^m x_{ij}^2}, (1 \leq i \leq m, 1 \leq j \leq n) \quad (2)$$

4.2.3. Step-3: Positive and negative ideal solutions

Positive and negative ideal solution is determined in Step-3. As described in [Table 2](#), the positive ideal solution for scenario-1 having highest bulk density (Max.), lowest water absorption (Min.) and highest compressive strength (Max.) and the negative ideal solution is vice versa. Positive and negative ideal solution is calculated for all scenarios by following Eq. (3) and (4), respectively.

$$\begin{aligned} A^+ &= \{ \langle \max(P_{ij} | i = 1, 2, \dots, m) | j \in N_b \rangle, \langle \min(P_{ij} | i = 1, 2, \dots, m) | j \in N_c \rangle \} \\ A^+ &= [a_1^+, a_2^+, \dots, a_n^+] \end{aligned} \quad (3)$$

$$\begin{aligned} A^- &= \{ \langle \min(P_{ij} | i = 1, 2, \dots, m) | j \in N_b \rangle, \langle \max(P_{ij} | i = 1, 2, \dots, m) | j \in N_c \rangle \} \\ A^- &= [a_1^-, a_2^-, \dots, a_n^-] \end{aligned} \quad (4)$$

4.2.4. Step-4: Separation of ideal solutions

Positive and negative solutions separated by making positive separation matrix (5) and negative separation matrix (6)

$$D^+ = \left[\sqrt{\sum_{j=1}^n (P_{ij} - a_j^+)^2} \right] \quad (5)$$

$$D^- = \left[\sqrt{\sum_{j=1}^n (P_{ij} - a_j^-)^2} \right] \quad (6)$$

Table 5

Normalization for decision matrix for MCDM.

Days (d)	Group	Criteria			Normalized			Remark
		Density	Water absorption	Strength	Density	Water absorption	Strength	
7	I	1,672	15.2	17.7	0.40	0.46	0.26	Group-I-7d
	II	1,797	15.8	17.0	0.43	0.47	0.25	Group-II-7d
	III	1,634	15.0	28.6	0.40	0.45	0.42	Group-III-7d
28	I	1,628	14.1	22.7	0.39	0.42	0.34	Group-I-28d
	II	1,728	13.5	24.1	0.42	0.41	0.36	Group-II-28d
	III	1,656	4.7	45.3	0.40	0.14	0.67	Group-III-28d

Table 6

Summary of RCC and rank for each alternative in each scenario.

Alternative	Scenario-1		Scenario-2		Scenario-3	
	RCC	Rank	RCC	Rank	RCC	Rank
Group-I-7d	0.044	6	0.956	1	0.565	6
Group-II-7d	0.554	4	0.942	2	0.664	3
Group-III-7d	0.579	3	0.793	5	0.629	4
Group-I-28d	0.551	5	0.870	3	0.668	2
Group-II-28d	0.584	2	0.837	4	0.674	1
Group-III-28d	0.944	1	0.552	6	0.593	5

4.2.5. Step-5: Calculation of relative closeness coefficient

TOPSIS is basically a distance-based approach, from the set ideal positive and negative solutions the shortest distance from positive ideal solution determined the best alternative Therefore, relative closeness

coefficient (RCC) is determined from Eq. (7)

$$RCC = \frac{D_i^-}{D_i^+ + D_i^-} \quad (7)$$

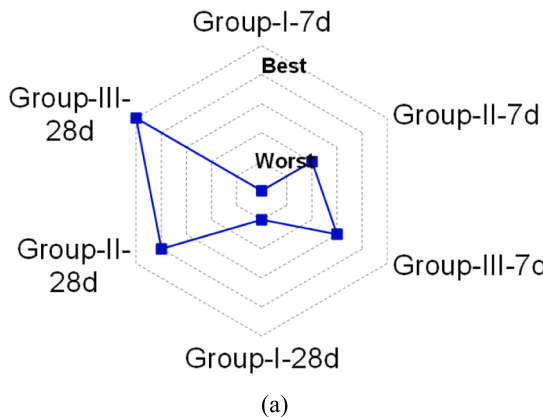
4.2.6. Step-6: Ranking

The values of RCC for each alternative is calculated from Eq. (7) and the highest value set as Rank 1 and lowest value has the least priority among all alternatives.

4.3. Assessment for performance scenario

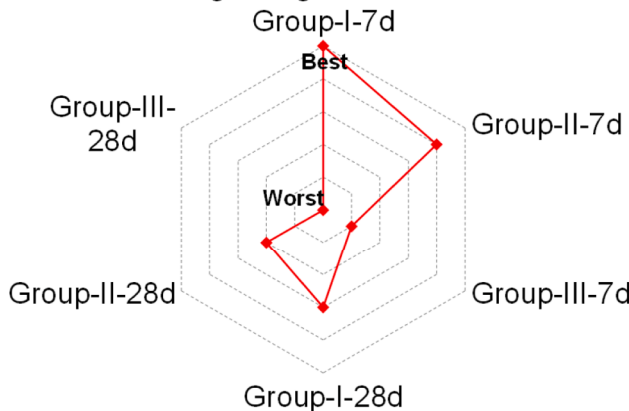
Automated selection was performed using TOPSIS, as described in Steps 1–6 in Section 4.1. The decision matrix was established as shown in Table 5. All criteria values for each group were obtained from experimental observations, as described in Section 3. A matrix with six

■ Scenario-1: High Strength of Durability



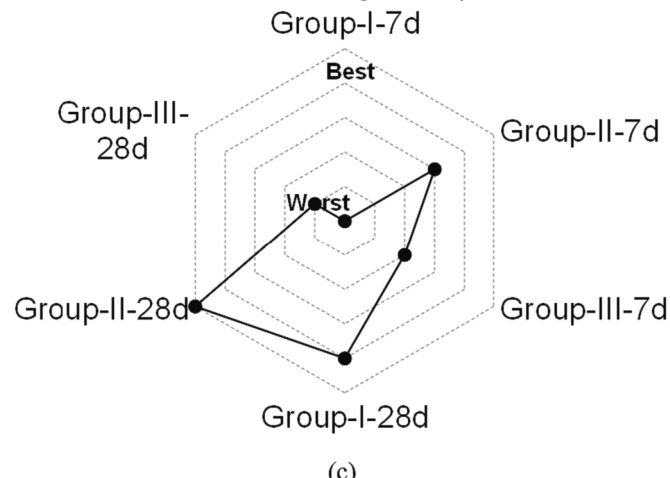
(a)

◆ Scenario-2: Lightweight of Thermal Insulation



(b)

● Scenario-3: Strength Requirement



(c)

Fig. 14. Analytical priorities of construction brick based on RCC results: (a) Scenario-1, (b) Scenario-2, and (c) Scenario-3.

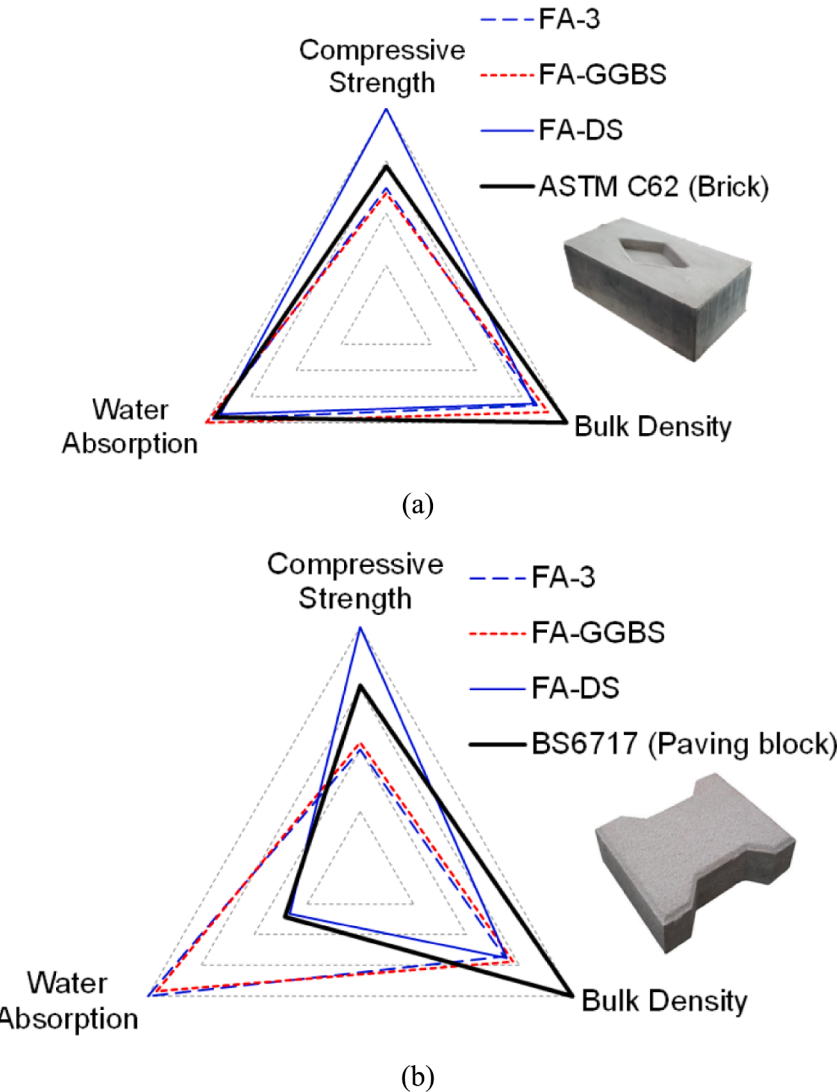


Fig. 15. Experimental selection of brick and paving brick from all group: (a) Construction brick and (b) Paving brick.

rows and three columns was created as the decision matrix (Eq. (1)), and its normalized values, obtained using Eq. (2), are listed in Table 5. Positive and negative calculations for an ideal solution were investigated, based on the description presented in Section 4.1, and their corresponding matrices were separated. The RCC values and their rankings are listed in Table 6. The geopolymer-based alternatives that were developed were selected based on three scenarios. In each scenario, all alternatives were compared with respect to the physico-mechanical performance criteria (Fig. 14). Scenario-1 represents high durability, characterized by maximum bulk density, minimal water absorption, and maximum compressive strength. The specimen that best exemplified this scenario was Group-III-28d. The priority of each specimen is plotted in Fig. 14(a). Group-I-7d demonstrated the worst performance. However, the Group-III specimens were the first and third choices when sustainable construction materials with high durability were required.

Fig. 14(b) presents the case of Scenario-2, where lightweight thermal insulation was prioritized. In this scenario, the lowest values of the bulk density, compressive strength, and maximum water absorption criteria were selected. The priority of each specimen is shown in Fig. 14(b). Group-I-7d was the best option, followed by Group-II-7d. This ranking order corresponds to the curing age of 28 d. Fig. 14(c) presents Scenario-3, where the lowest values of bulk density, water absorption, and

concrete strength were selected. For this scenario, the first option was Group-II-28d, followed by the result of Group-I-28d. Typically, Scenario-3 is used for formulating a control-required strength material that has wide applicability for both structural and non-structural applications.

4.4. Appraisal of design specification for construction brick

The priority of each criterion (bulk density, water absorption, and compressive strength) for each group is described in Fig. 15. The values of bulk density (less than $2,000 \text{ kg/m}^3$), water absorption (less than 15 %), and compressive strength (20.5 MPa) under severe weathering conditions are presented in ASTM C62 [52]. All values were plotted after normalization, as shown in Fig. 15(a). The bulk density values of all groups were less than those specified by the code and acceptable, whereas the water absorption value was within an acceptable range; however, the strength of FA-DS was only acceptable for severe weathering conditions at 7 d. Meanwhile, the values indicated by FA-3 and FA-GGBS were only acceptable under moderate or no weathering conditions. The results at 28 d indicate that all groups fulfilled the physico-mechanical performance and can be used to fabricate brick masonry bricks for arid regions.

Similarly, Fig. 15(b) presents a comparison of the selected paving

bricks, where the required strength was approximately 45 MPa. The normalized values for paving bricks specified in BS 6717 [58] and the normalized values of all groups at 28 d are plotted in Fig. 15(b). The bulk density was less than that specified in the codes (approximately 2,400 kg/m³); however, the targeted strength was only achieved by the DS incorporated AAB mixture.

5. Conclusions

In this study, an AAB was designed to synthesize geopolymer construction bricks. To enable a wide application of those bricks in Arid region, DS incorporated mixtures with FA and GGBS were investigated. The application of the construction brick was assessed based on the physico-mechanical performance. The optimum types of AAB mixtures were determined in an arid region using the MCDM technique, and the following conclusions were inferred:

1. The compressive strength was correlated with the FA type, and its values varied from 9.6 to 22.7 MPa. However, the difference in compressive strength between 7 and 28 d was marginal because of the early geopolymerization via hot curing. Furthermore, the SAI for the three types of FAs was calculated, and the FA with the highest SAI (1.86) was used to develop GGBS and DS based AAB mixtures.
2. Among all specimens, the DS incorporated AAB mixture exhibited the highest compressive strength (45.3 MPa). This was enabled by hot curing, which can significantly improve the reactivity of FA and DS (as precursors) during geopolymerization. Hence, high-strength materials based on DS for arid regions can be achieved.
3. The bulk density of the developed AAB mixture varied from 1,609 to 1,762 kg/m³, and the DS incorporated specimens had a lower density than the GGBS incorporated AAB mixture. In fact, the DS incorporated specimens was significantly less dense than conventional concrete (2,200–2,400 kg/m³) and fired clay brick (1,800–2,000 kg/m³). Thus, they can make lighter members.
4. The water absorption of the DS incorporated AAB mixture was 4.5 %, whereas that of the FA-based and GGBS incorporated AAB mixtures was approximately 14 % at 28 d. DS incorporation can result in a porous less lightweight construction material.
5. MCDM analysis results according to performance-based scenario, it was revealed that only FA-based binder is suitable for lightweight and thermal insulation applications. FA + DS mixture is the optimum AAB for high strength and durability scenarios and is suitable for paving blocks.

Declaration of Competing Interest

The authors declare that they have no known competing financial interests or personal relationships that could have appeared to influence the work reported in this paper.

Acknowledgments

The authors extend their appreciation to the Deanship of Scientific Research at Imam Mohammad Ibn Saud Islamic University for funding this work through Research Group No. RG-21-12-05.

References

- [1] T. Luukkonen, Z. Abdollahnejad, J. Yliniemi, P. Kinnunen, M. Illikainen, One-part alkali-activated materials: a review, *Cem. Concr. Res.* 103 (2018) 21–34.
- [2] C. Ma, G. Long, Y. Shi, Y. Xie, Preparation of cleaner one-part geopolymer by investigating different types of commercial sodium metasilicate in China, *J. Clean. Prod.* 201 (2018) 636–647.
- [3] J.L. Provis, Cement and concrete research alkali-activated materials, *Cem. Concr. Res.* 114 (2018) 40–48.
- [4] M. Refaat, A. Mohsen, E.S.A.R. Nasr, M. Kohail, Minimizing energy consumption to produce safe one-part alkali-activated materials, *J. Clean. Prod.* 323 (2021), 129137.
- [5] A. Yilmazoglu, S.T. Yildirim, Ö.F. Behçet, S. Yıldız, Performance evaluation of fly ash and ground granulated blast furnace slag-based geopolymers concrete: a comparative study, *Struct. Concr.* 23 (2022) 3898–3915.
- [6] Z. Kurt, Novel Binder Material in Geopolymer Mortar Production: Obsidian Stone Powder (2023) 1–14.
- [7] F. Koksal, O.Y. Bayraktar, B. Bodur, A. Benli, G. Kaplan, Insulating and fire-resistant performance of slag and brick powder based one-part alkali-activated lightweight mortars, *Struct. Concr.* 1–19 (2022).
- [8] M.G.M. Elipe, S. López-Querol, Aeolian sands: characterization, options of improvement and possible employment in construction - the state-of-the-art, *Constr. Build. Mater.* 73 (2014) 728–739.
- [9] A.S. Al-Harthi, M.A. Halim, R. Taha, K.S. Al-Jabri, The properties of concrete made with fine dune sand, *Constr. Build. Mater.* 21 (2007) 1803–1808.
- [10] A. Belferra, A. Krikor, S. Abboudi, S.T. Bi, Effect of granulometric correction of dune sand and pneumatic waste metal fibers on shrinkage of concrete in arid climates, *J. Clean. Prod.* 112 (2016) 3048–3056.
- [11] K. Rashid, S. Farooq, A. Mahmood, S. Iftikhar, A. Ahmad, Moving towards resource conservation by automated prioritization of concrete mix design, *Constr. Build. Mater.* 236 (2020), 117586.
- [12] W.L. Tan, Y.H. Lee, C.S. Tan, Y.Y. Lee, A.B.H. Kueh, Mechanical properties and fracture prediction of concretes containing oil palm shell and expanded clay for full replacement of conventional aggregates, *J. Teknol.* 84 (2022) 171–181.
- [13] M. He, Y. Wang, K. Yuan, Z. Sheng, J. Qiu, J. Liu, J. Wang, Synergistic effects of ultrafine particles and graphene oxide on hydration mechanism and mechanical property of dune sand-incorporated cementitious composites, *Constr. Build. Mater.* 262 (2020), 120817.
- [14] J. Kaufmann, Evaluation of the combination of desert sand and calcium sulfoaluminates cement for the production of concrete, *Constr. Build. Mater.* 243 (2020), 118281.
- [15] Y. Liu, Y. Li, G. Jiang, Orthogonal experiment on performance of mortar made with dune sand, *Constr. Build. Mater.* 264 (2020), 120254.
- [16] M. Verma, N. Dev, Effect of ground granulated blast furnace slag and fly ash ratio and the curing conditions on the mechanical properties of geopolymers concrete, *Struct. Concr.* 23 (2022) 2015–2029.
- [17] N.B. Singh, B. Middendorf, Geopolymers as an alternative to Portland cement: an overview, *Constr. Build. Mater.* 237 (2020), 117455.
- [18] C. Kuenzel, N. Ranjbar, Dissolution mechanism of fly ash to quantify the reactive aluminosilicates in geopolymers, *Resour. Conserv. Recycl.* 150 (2019), 104421.
- [19] I. Zafar, K. Rashid, S. Tariq, A. Ali, M. Ju, Integrating technical-environmental-economical perspectives for optimizing rubber content in concrete by multi-criteria analysis, *Constr. Build. Mater.* 319 (2022) 1–16.
- [20] L.T. Tay, Y.Y. Lee, Y.H. Lee, A.B.H. Kueh, A review on the behaviour, properties and favourable characteristics for thermally insulated concrete for tropical climate, *J. Eng. Sci. Technol.* 17 (2022) 1608–1643.
- [21] M. Ahmad, K. Rashid, Z. Tariq, M. Ju, Utilization of a novel artificial intelligence technique (ANFIS) to predict the compressive strength of fly ash-based geopolymers, *Constr. Build. Mater.* 301 (2021), 124251.
- [22] W. Lokuge, A. Wilson, C. Gunasekara, D.W. Law, S. Setunge, Design of fly ash geopolymers concrete mix proportions using multivariate adaptive regression spline model, *Constr. Build. Mater.* 166 (2018) 472–481.
- [23] I. Zafar, K. Rashid, R. Hameed, K. Aslam, Correlating Reactivity of Fly Ash with Mechanical Strength of the Resultant Geopolymer, *Arab. J. Sci. Eng.* 2022.
- [24] S.F. Ali Shah, B. Chen, M.R. Ahmad, M.A. Haque, Development of cleaner one-part geopolymers from lithium slag, *J. Clean. Prod.* 291 (2021), 125241.
- [25] S. Hosseini, N.A. Brake, M. Nikookar, Ö. Günaydin-Şen, H.A. Snyder, Mechanochemically activated bottom ash-fly ash geopolymers, *Cem. Concr. Compos.* 118 (2021), 103976.
- [26] F. Matalkah, L. Xu, W. Wu, P. Soroushian, Mechanochemical synthesis of one-part alkali aluminosilicate hydraulic cement, *Mater. Struct. Constr.* 50 (2017) 1–12.
- [27] H.A. Abdel-Gawwad, K.A. Khalil, Application of thermal treatment on cement kiln dust and feldspar to create one-part geopolymers cement, *Constr. Build. Mater.* 187 (2018) 231–237.
- [28] M.B. Hossain, M. Roknuzzaman, M.A. Biswas, M. Islam, Evaluation of engineering properties of thermal power plant waste for subgrade treatment, *J. Civ. Eng. Sci. Technol.* 12 (2021) 112–123.
- [29] Z.Y. Lau, S.L. Lee, M. Abdul Mannan, G.S. Slavcheva, C. Oucif, Performance of polymer grouts made from wastes for permeable rigid pavement connections, *J. Civ. Eng. Sci. Technol.* 13 (2022) 150–159.
- [30] M.M. Mimi, A. Shakil, R. Haque, R. Hasan, Effect of Addition of CaO on Compressive Strength of High-Volume Fly Ash Concrete 14 (2023) 64–76.
- [31] W.Q. Chin, Y.H. Lee, M. Amran, R. Fediuk, N. Vatin, A.B.H. Kueh, Y.Y. Lee, A sustainable reuse of agro-industrial wastes into green cement bricks, *Materials (Basel)*, 15 (2022).
- [32] M. Ahmad, K. Rashid, Novel approach to synthesize clay-based geopolymers brick: optimizing molding pressure and precursors' proportioning, *Constr. Build. Mater.* 322 (2022), 126472.
- [33] M. Ahmad, K. Rashid, R. Hameed, E. Ul Haq, H. Farooq, M. Ju, Physico-mechanical performance of fly ash based geopolymers brick: Influence of pressure – temperature – time, *J. Build. Eng.* 50 (2022), 104161.
- [34] M. Gonçalves, I.S. Vilarinho, M. Capela, A. Caetano, R.M. Novais, J.A. Labrincha, M.P. Seabra, Waste-based one-part alkali activated materials, *Materials (Basel)*, 14 (2021) 1–17.
- [35] A. Hajimohammadi, J.S.J. van Deventer, Characterisation of one-part geopolymers binders made from fly ash, *Waste Biomass Valoriz.* 8 (2017) 225–233.

- [36] B. Nematollahi, J. Sanjayan, F.U.A. Shaikh, Synthesis of heat and ambient cured one-part geopolymers mixes with different grades of sodium silicate, *Ceram. Int.* 41 (2015) 5696–5704.
- [37] P. Sturm, G.J.G. Gluth, H.J.H. Brouwers, H.C. Kühne, Synthesizing one-part geopolymers from rice husk ash, *Constr. Build. Mater.* 124 (2016) 961–966.
- [38] W. Lv, Z. Sun, Z. Su, Study of seawater mixed one-part alkali activated GGBFS-fly ash, *Cem. Concr. Compos.* 106 (2020), 103484.
- [39] B.S. Mohammed, S. Haruna, M.M.A. Wahab, M.S. Liew, A. Haruna, Mechanical and microstructural properties of high calcium fly ash one-part geopolymers cement made with granular activator, *Heliyon*. 5 (2019) e02255.
- [40] C. Ma, B. Zhao, S. Guo, G. Long, Y. Xie, Properties and characterization of green one-part geopolymers activated by composite activators, *J. Clean. Prod.* 220 (2019) 188–199.
- [41] I. Zafar, K. Rashid, M. Ahmad, M. Ltifi, Thermo-chemico-mechanical activation of bagasse ash to develop geopolymers based cold-pressed block, *Constr. Build. Mater.* 352 (2022), 129053.
- [42] Astm C989., Standard specification for slag cement for use in concrete and mortars, ASTM International 2018 West Conshohocken, PA, USA.
- [43] Astm C618., Standard specification for coal fly ash and raw or calcined natural pozzolan for use in concrete 2019 West Conshohocken, PA.
- [44] I. Zafar, M.A. Tahir, R. Hameed, K. Rashid, M. Ju, Reactivity of aluminosilicate materials and synthesis of geopolymers mortar under ambient and hot curing condition, *Adv. Concr. Constr.* 13 (2022) 71–81.
- [45] R. Sharafudeen, J.M. Al-Hashim, M.O. Al-Harbi, A.I. Al-Ajwad, A.A. Al-Waheed, Preparation and characterization of precipitated silica using sodium silicate prepared from saudi arabian desert sand, *Silicon* 9 (2017) 917–922.
- [46] B.S. En 12390-7:2009, Testing hardened concrete. Density of hardened concrete 2009 London, UK.
- [47] Astm C20., Standard test methods for apparent porosity, water absorption, apparent specific gravity, and bulk density of burned refractory brick and shapes by boiling water, ASTM International 2015 West Conshohocken, PA, USA.
- [48] Astm C109., Standard test method for compressive strength of hydraulic cement mortars (Using 2-in. or [50 mm] Cube Specimens), ASTM International 2021 West Conshohocken, PA, USA.
- [49] Astm C311., Standard test methods for sampling and testing fly ash or natural pozzolans for use in portland-cement concrete, ASTM International 2018 West Conshohocken, PA, USA.
- [50] O. Shee-Ween, H. Cheng-Yong, L. Yun-Ming, M.M.A.B. Abdullah, H. Li Nghee, L.W. L. Chan, O. Wan-En, N.A. Jaya, N. Yong-Sing, Cold-pressed fly ash geopolymers: effect of formulation on mechanical and morphological characteristics, *J. Mater. Res. Technol.* 15 (2021) 3028–3046.
- [51] M.V. Deepthi, M. Sharma, R.R.N. Sailaja, P. Anantha, P. Sampathkumaran, S. Seetharamu, Mechanical and thermal characteristics of high density polyethylene-fly ash Cenospheres composites, *Mater. Des.* 31 (2010) 2051–2060.
- [52] Astm C62., Standard specification for building brick (Solid masonry units made from clay or shale) ASTM International 2017 West Conshohocken, PA, USA.
- [53] K. Rashid, E.U. Haq, M.S. Kamran, N. Munir, A. Shahid, I. Hanif, Experimental and finite element analysis on thermal conductivity of burnt clay bricks reinforced with fibers, *Constr. Build. Mater.* 221 (2019) 190–199.
- [54] M.U. Rehman, M. Ahmad, K. Rashid, Influence of fluxing oxides from waste on the production and physico-mechanical properties of fired clay brick: a review, *J. Build. Eng.* 27 (2020), 100965.
- [55] K.S. Al-Jabri, A.W. Hago, A.S. Al-Nuaimi, A.H. Al-Saidy, Concrete blocks for thermal insulation in hot climate, *Cem. Concr. Res.* 35 (2005) 1472–1479.
- [56] A.B.H. Kueh, A.W. Razali, Y.Y. Lee, S. Hamdan, I. Yakub, N. Suhaili, Acoustical and mechanical characteristics of mortars with pineapple leaf fiber and silica aerogel infills – measurement and modeling, *Mater. Today Commun.* 35 (2023), 105540.
- [57] S. Iftikhar, K. Rashid, E. Ul Haq, I. Zafar, F.K. Alqahtani, M. Iqbal Khan, Synthesis and characterization of sustainable geopolymers green clay bricks: an alternative to burnt clay brick, *Constr. Build. Mater.* 259 (2020), 119659.
- [58] BS-6717, Precast, Unreinforced Concrete Paving Blocks - Requirements and Test Methods, British Standards Institution, London, UK, 2001.
- [59] K. Rashid, A. Yazdanbakhsh, M.U. Rehman, Sustainable selection of the concrete incorporating recycled tire aggregate to be used as medium to low strength material, *J. Clean. Prod.* 224 (2019) 396–410.